Nanoscale

Accepted Manuscript

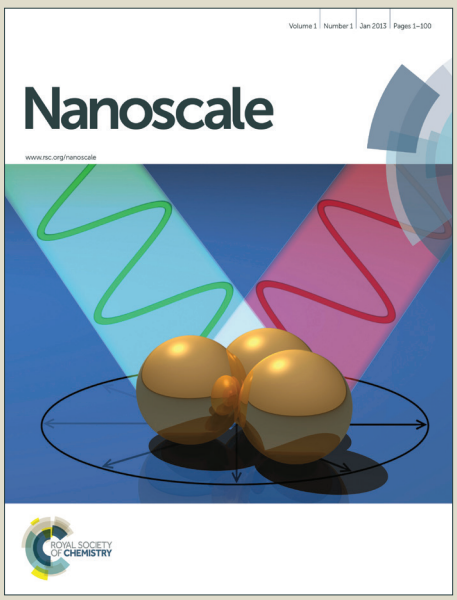

This is an *Accepted Manuscript*, which has been through the Royal Society of Chemistry peer review process and has been accepted for publication.

Accepted Manuscripts are published online shortly after acceptance, before technical editing, formatting and proof reading. Using this free service, authors can make their results available to the community, in citable form, before we publish the edited article. We will replace this *Accepted Manuscript* with the edited and formatted *Advance Article* as soon as it is available.

You can find more information about *Accepted Manuscripts* in the Information for Authors.

Please note that technical editing may introduce minor changes to the text and/or graphics, which may alter content. The journal's standard Terms & Conditions and the Ethical guidelines still apply. In no event shall the Royal Society of Chemistry be held responsible for any errors or omissions in this *Accepted Manuscript* or any consequences arising from the use of any information it contains.

ROYAL SOCIETY OF CHEMISTRY

www.rsc.org/nanoscale

Graphical Abstract

We developed dual pH-sensitive fluorescent dyes-loaded polypeptide nanoparticles (DPNs) for ratiometric sensing of pH changes. DPNs have good pH responses for solution and cells. Single acid activatable fluorescent dye doped polypeptide nanoparticles can distinguish tumor tissue from normal tissue by monitoring the extracellular acidification environment.

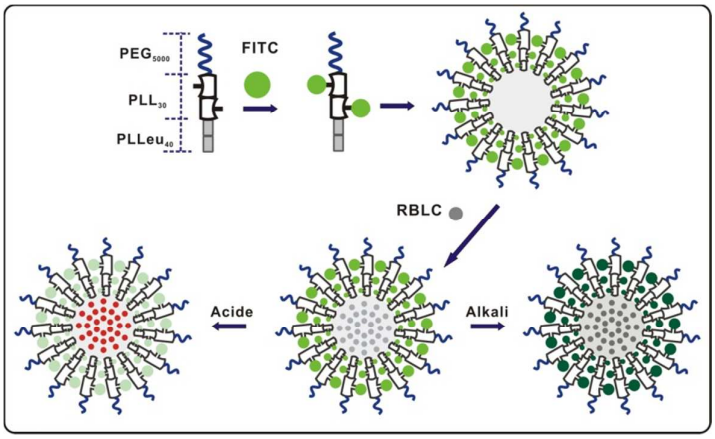

Nanoscale Accepted Manuscript

Cite this: DOI: 10.1039/c0xx00000x

www.rsc.org/xxxxxx

ARTICLE TYPE

Polypeptide micelles with dual pH activable dyes for sensing cells and cancer imaging

Ping Gong†, Yueting Yang†, Huqiang Yi, Shengtao Fang, Pengfei Zhang, Zonghai Sheng, Guanhui Gao, Duyang Gao, and Lintao Cai*

Received (in XXX, XXX) Xth XXXXXXXXX 20XX, Accepted Xth XXXXXXXXX 20XX
DOI: 10.1039/b000000x

pH is an important control parameter for maintenance of cell viability and tissue functions. The pH monitoring provides valuable information on cell metabolic processes and living environment. In this study, we prepared dual pH-sensitive fluorescent dyes-loaded polypeptide nanoparticles (DPNs) for ratiometric sensing of pH changes in living cells. DPNs contain two types of dyes: N-(rhodamine B) lactam cystamine (RBLC), an acid activatable fluorescent dye with fluorescence increased in acidic environment and fluorescein isothiocyanate (FITC), while a base activatable fluorescent dye with fluorescence enhanced in alkaline environment. Hence, DPNs exhibited dual response signal with strong red fluorescence and weak green fluorescence under acidic conditions; on the contrary, they showed strong green fluorescence and almost no red fluorescence at alkaline and neutral conditions. The favorable inverse pH responses of two fluorescence dyes resulted in ratiometric pH determination for DPNs with optimized pH-sensitive range of pH 4.5-7.5. Quantitative analysis of intracellular pH of intact MCF-7 cells have been successfully demonstrated with our nanosensor. Moreover, single acid activatable fluorescent dye doped polypeptide nanoparticles that only loaded RBLC can distinguish tumor tissue from normal tissue by monitoring the extracellular acidification environment.

Introduction

pH is important in regulating the nature and rate of chemical reactions necessary to support life. pH modulates the function of many organelles and plays a pivotal role in cell metabolism processes, such as the proliferation and apoptosis [1-3]. The mammalian cell has therefore been equipped to maintain a normal pH in response to enviromental changes and metabolic acid generation. In humans, the blood acidity must remain in this narrow range in order to maintain normal enzyme, cell function and metabolism.[4, 5].

It has been stated in the literature that the pH of acutely inflamed and infected tissue, triggering solid tumor became acidic. The inflammatory response can reduce local pH to 5.5 or lower due to the damaged vasculature and the release of various enzymes during phagocytosis [6]. Solid tumors tend to have a more acidic extracellular microenvironment than normal tissues due to a combination of more glycolytic phenotype, as well as reduced oxygen availability, leading to lactic acidosis from glycolysis [7-10]. Intratumoral acidosis was reported to associate with tumorigenic transformation, resistance to chemotherapies, up-regulation of angiogenesis and metastasis [11, 12]. Furthermore, neutralization of the tumor microenvironment can inhibit the metastasis and increase the response to therapies [13-15].

Therefore, it is essental for monitoring pH distribution and fluctuation with high temporal–spatial resolution in living cells and body [16]. Towards this end, great efforts have been explored to develop pH sensors. Small molecular fluorescent probes as well as fluorescent proteins have been widely used for intracellular pH (pHi) detection [17-24]. Recently, nanoparticle-based ratiometric pH sensors have attracted more and more attention owing to their remarkable advantages [25-29]. The most important of these being that it is easy to simultaneously assemble diverse dyes (usually pH-sensitive and pH-insensitive) on the same nanoparticle to acquire ratiometric fluorescent sensors with tunable pH response range. A number of fluorescent nanosensors, based on silicon, polymers, or quantum dots, have been designed to quantify intracellular pH [29-31].

The pH of human inflamed and tumor tissues has been measured by a variety of techniques [32-38]. The most traditional technique is the use of pH-sensitive electrodes with tip diameters ranging from 0.5 pm to 2 mm. However, it is invasive to destroy the membrane integrity, moreover large electrodes can affect tumor microcirculation and the cellular metabolic microenvironment. Additional, since the measurements are based on the potentiometric technique, thus pH data obtained with electrodes is generally accepted to mainly represent the hydrogen ion activity rather than the H^+ concentration.[8]. Other strategies such as via ^{31}P and ^{1}H magnetic resonance spectroscopy (MRS) were adopted to detect pH distribution [32]. But theapplications were limited due to expensive costand low sensitivity of MRS, which only allowed to evaluate extracellular pH (pHe) from relatively large tissue volumes.

Here, we developed dual pH-sensitive fluorescent dyes-loaded polypeptide nanoparticles (DPNs) for ratiometric sensing of pH changes in living cells. Firstly, DPNs were prepared by self-assembling of copolymers. Then pH response of DPNs to solution was evaluated. Quantitative determinations of

Nanoscale Accepted Manuscript

intracellular pH of intact MCF-7 cells were performed with the nanosensor. And the cytotoxicity of DPNs to cells was invetigated. Futhermore, single acid activatable fluorescent dye doped polypeptide nanoparticles that only packed RBLC (RPNs) were also applied to image tumor tissue by monitoring the extracellular acidification environment.

Experimental

Chemicals and materials

O-(2-Aminoethyl)-O'-(2-methyl) polyethylene glycol (PEG-NH2, Mw = 5000), Trifluoroacetic acid-d was purchased from Sigma-Aldrich (Natick, MA). L-Leucine (LLeu) and ε-benzyloxycarbonyl-L-lysine (LLZ) were purchased from GL Biochem (Shanghai, China) and recrystallized from ethyl acetate three times. Hydrogen bromide 33 wt% solution in glacial acetic acid was purchased from ACROS Organics. Tetrahydrofuran (THF) and n-hexane were provided by Shanghai Chemical Reagent China and dried with sodium before use. fluorescein isothiocyanate (FITC) and Rhodamine B were purchased from Shanghai Apeptide CO. LTD. N,N,N-Triethylamine (TEA), Triphosgene, N, N'-Dimethylformamide (DMF) and dimethylsulfoxide (DMSO) were provided by J&K Scientific, Triphosgene was recrystallized from diethyl ether before use, DMF and DMSO were distilled under reduced pressure before use. NCarboxyanhydride (NCA) of ε-benzyloxycarbonyl-L-lysine (LLZNCA) and N-carboxyanhydride of L-Leucine (LLeu-NCA) were prepared according to the method of Daly and Poché. [39] All other solvents were obtainedfrom Shanghai Chemical Reagent China and used without further purification. 3-(4,5-dimethylthiazol-2-yl)-2,5-diphenyl-tetrazolium bromide (MTT), LysoTracker Blue DND-22, nigericin, DMEM medium, fetal bovine serum (FBS) and kanamycin sulfate were purchased from Invitrogen Co. Ltd. Other chemicals if not specified were all commercially available and used as received. MCF-7 and H460 cells were kindly provided by the Cell Center of our institute.

The buffer solutions were as follows: the high K^+ buffer buffer containing 30 mM NaCl, 6 120 mM KCl, 1 mM $CaCl_2$, 0.5 mM $MgSO_4$, 1 mM NaH_2PO_4, 5 mM glucose, 20 mM HEPES (various pH values was adjusted used NaOH); phosphate buffered saline solution (PBS) containing 137 mM NaCl, 2.7 mM KCl, 4.3 mM Na_2HPO_4, 1.4 mM KH_2PO_4 (pH 7.4).

Preparation and characterization of N-(rhodamine B) lactam cystamine (RBLC)

Firstly, we synthesized 2-Boc-aminoethyldithio-2'-ethylamine hydrochloride (mono-Boc-cystamine) as previous paper reported [40]. Then, mono-Boc-cystamine (315 mg, 1.25 mmol), Rhodamine B (479 mg, 1 mmol), N, N–dicyclohexylcarbodiimide (DCC, 226 mg, 1.1 mmol), 4-dimethylamiopryidine (DMAP, 24.4 mg, 0.2 mmol) were dissolved in CH_2Cl_2 (30 mL) and refluxed for about 6 h, the reaction was monitored by thin layer chromatography (TLC). After stirring for 6 h, the reaction was stopped and concentrated under vacuum to afford crude product rhodamine B-cystamine-Boc(3). It was further purified by column chromatography, yield 50%. Then above product (160 mg, 0.236 mmol)was dissolved with 3mL CF_3COOH in the ice bath, then stirred for 1 h at room temperature. After removing the solvent, the residue was dissolved in CH_2Cl_2 and extracted with 0.2 M NaOH (3×20 mL), following extracting with H_2O (2×20 mL) to remove the salt. The organic layer was combined and evaporated to afford the crude product N-(rhodamine B) lactam cystamine (RBLC). The next purification depended on column chromatography on silica gel flash chromatography using CH_2Cl_2/EtOH as eluent. Finally, the desired product was obtained as an pink solid, yield 90%. The product was confirmed by ^{1}HRMS and mass spectrum. (Fig. S2 and S3).

Preparation and characterization of PEG-PLL-PLLeu and PEG-PLL-PLLeu-FITC

the triblock polypeptide copolymers as PEG-PLL_{30}-$PLLeu_{40}$ (the subscript number represents degree of polymerlzation of each block) were designed as shown in Fig. 1A following our previously reported procedure [41]. In brief, the PEG-PLLZ copolymers were synthesized by ring-opening polymerization of N-Carboxyanhydride (NCA) of ε-benzyloxycarbonyl-L-lysine (LLZ-NCA) using PEG_{2000}-NH_2 as initiator, then PEG-PLL_{30}-$PLLeu_{40}$ copolymers was preparedby further ring-opening polymerization of LLeu-NCA initiated by PEG-PLLZ. The product (PEG-PLLZ-PLLeu) was precipitated using diethyl ether and purified by repeated precipitation in diethyl ether, then dried in a vacuum. PEG-PLL-PLLeu copolymers were obtained by the deprotection of PEG-PLLZ-PLLeu. Proton nuclear magnetic resonance (^{1}H NMR) spectra were recorded on a Bruker 400 MHz nuclear magnetic resonance instrument using Trifluoroacetic acid-d as the solvents. Fourier-transform infrared spectra (FT-IR) spectrums of PEG-PLLZ-PLLeu and PEG-PLL-PLLeu copolymers were obtained by a Frontier™ spectrometer. And the apparent molecular weight of each PEG-PLL-PLLeu was determined by Gel Permeation Chromatography (VE2001 GPCmax, Malven Company)

PEG-PLL-PLLeu-FITC was synthesized by directly coupling of FITC to the amino group of PEG-PLL-PLLeu. Typically, 0.1 mg FITC in 1 mL DMSO was mixed with 1.3 mL 2.6 mg/mL PEG-PLLZ-PLLeu in DMSO, and then 2μL TEA was added. The reaction mixture was stirred for 12 hours at room temperature. Finally, PEG-PLL-PLLeu-FITC was obtained and used without further purification.

Preparation and characterization of Micelle NPs

The CMC of micelles self-assembled from PEG-PLL-PLLeu copolymers was determined according to the literature using pyrene as a hydrophobic fluorescent probe [42]. DPNs and RPNs were prepared by dialyzing mixture of copolymers (PEG-PLL-PLLeu-FITC or PEG-PLL-PLLeu) with RBLC dissolving in DMSO using dialysis bag in water as shown in scheme 1B. 2.6 mg PEG-PLL-PLLeu or 2.7 mg PEG-PLL-PLLeu-FITC was mixed with 0.2 or 0.5 mg RBLC in DMSO solution, then the mixture was dialyzed in water with magnetic stirring for 12 h. About 4.5 mL micelle NPs in water were obtained.The particle size and zeta potential were measured from three repeated experiments via dynamic light scattering (DLS) using a Malvern Zetasizer Nano-ZS90 (Malvern instruments, UK). All of the DLS measurements were performed at 25°C and at a scattering angle 90°. Transmission electronic microscopic (TEM) imagings were performed using Tecnai G2 F20 S-TWIN (FEI Company, American).

Fluorescence measurement

The fluorescence spectra were investigated on a FSP920 spectrofluorometer (Edinburgh Instruments, English). The excitation and emission monochromator slits were both set to 2

Nanoscale Accepted Manuscript

This journal is © The Royal Society of Chemistry [year]

nm, 3 nm, respectively. For the fluorescence emission spectra, the excitation wavelength (λex) for FITC and RBLC was set to 488 nm and 550 nm , respectively. To measure the variation of fluorescent intensity of nanoparticles with time, the λex was set to the same wavelength mentioned above and the emission wavelength (λem) was set to 667 nm.

Cell culture and fluorescence imaging

Cells were cultured in DMEM medium containing 10% fetal bovine serum (FBS), 100 U/mL penicillin and 100 μg/mL streptomycin in a humidified atmosphere with 5% CO_2 at 37 °C. The cells were maintained in an exponential growth phase by periodic subcultivation. The cell density was determined using a hemocytometer, and this was performed prior to any experiments. MCF-7 cells for imaging were initially seeded in 35 mm glass bottom dishes (P35G-0-10-C, MatTek Corp.) at a density of 200,000 cells/well with medium containing 10% FBS overnight. For fluorescence imaging of cells treated with different pH buffer, cells were cultured with serum free media containing DPNs (0.05mg/mL) for 2 hours, and then washed with PBS for 2 time, incubating in the high K^+ buffer buffer of different pH containing nigericin (10 μM) for 10 minutes. Cells were captured by using Laser Scanning Confocal Microscope (LSCM, Leica TCS SP5). For lysosome imaging, cells were washed twice with the preheated PBS and incubated in serum free medium. And then followed by addition of LysoTracker Blue DND 22 (1 μM) and DPNs (10 μg/mL). The cells were further incubated for 30 minutes. The media were removed and replaced with fresh serum free media. Cells were then analyzed with confocal fluorescence microscope.

Cytotoxicity assay

The cytotoxicity of DPNs and RPNs was evaluated by the standard MTT assay. Briefly, MCF-7 cells were seeded in 96 bottom microplates at a density of 7000 cells/well, and incubated with micelle NPs at varied concentrations (0-80 μg/mL) at 37°C for 24 h. Then, the culture media were discarded, and 0.1 mL of the MTT solution (0.5 mg/ mL in DMEM) was added to each well, followed by incubation at 37°C for 4 h. The supernatant was abandoned, and 110 μL of DMSO was added to each well to dissolve the formed formazan. After shaking the plates for 10 min, absorbance values of the wells were read with a microplate reader at 490 nm. The cell viability rate (VR) was calculated according to the equation: $VR = A/A_0 \times 100\%$, where A is the absorbance of the experimental group (i.e., the cells were treated by micelle NPs) and A_0 is the absorbance of the control group (i.e., the cells were untreated by micelle NPs).

Animals and tumor implantation

50 BALB/c nude mice were provided by Medical Experimental Animal Center of Guangdong Province. They were 4–6 weeks old at the start of each experiment and weighed 20-25 g. For tumor implantation, 30 nude mice received a subcutaneous injection of 5×10^6 H460 cells suspended in 0.2 mL of saline solution in the left hind limb. Tumors were then allowed to grow to 1-2 cm in diameter for 10–30 days. All animal operations were in according with institutional animal use and care regulations, approved by the Laboratory Animal Center of Guangdong.

***In Vivo* fluorescence imaging**

Before imaging, nude mice, with tumors, were anesthetized with an intraperitoneal (IP) injection of 70-100 mg⁄kg pentobarbital sodium. Once the mice were anesthetized to be motionless, a 150 μL volume of containing free RPNs was injected via the tail vein. At specified times, abdominal and dorsal region fluorescence images of of live mice or freshly removed tumor tissues and organs of treated mice were taken by a Maestro™ *in vivo* fluorescence imaging system (Cambridge Research & Instrumentation, Inc.). A 523 nm (± 25 nm) bandpass filter and a 560 nm longpass filter (560 to 740 nm) were selected to be used as the excitation filter and the emission filter, respectively.

Results and Discussion

Characteristics of copolymers and micelle NPs

The PEG-PLL-PLLeu copolymers were synthesized through three steps as show in Fig 1. Firstly, we prepared the diblock copolymer PEG-PLLZ by ring-opening polymerization of LLZ-NCA using mPEG-NH_2 as initiator. Then, the triblock copolymer PEG-PLLZ-PLLeu was synthesized by further ring-opening polymerization of LLeu-NCA using amino-terminated PEG-PLLZ as a macromolecular initiator. The amphiphilic PEG-PLL-PLLeu triblock copolymers were obtained after the deprotection of PEG-PLLZ-PLLeu by HBr/HAc in TFA solution. The ^{1}H NMR spectra of PEG-PLLZ-PLLeu and PEG-PLL-PLLeu were shown in Fig. 2. The peaks around 3.8 ppm were attributable to the protons ($-CH_2CH_2O$) in the PEG chain, and the peaks exhibited between 0.8 and 0.9 ppm were attributed to the protons ($-CH_3$) in PLLeu. The results of the FT-IR spectra in Fig. S1 furthermore confirmed the synthesis of PEG-PLL-PLLeu copolymers. The peaks at 1650 cm^{-1} and 1550 cm^{-1} represented the amide I bond and amide II bond in the polypeptide, respectively. There can be a peak at 1105 cm^{-1}, contributing to the C-O-C stretching vibration in the PEG segment. Additionally, the peak at 1710 cm^{-1} was attributed to the C-O stretching vibration of Z in the spectra of PEG-PLLZ-PLLeu, which completely disappeared in the spectra of PEG-PLL-PLLeu, confirming the complete deprotection of PEG-PLLZ-PLLeu. Mw and Mw of PEG-PLL-PLLeu was 10310 and 10636, respectively, and PDI of the polymer was 1.032 obtained by gel permeation chromatography (GPC).

One of reason for choosing PEG-PLL-PLLeu triblock copolymers as pH sensitive probe carrier was that dyes used in this paper had the opposite hydrophilic properties. It was impossible to embed them at the same time, hence one of their need to be coupled. The reactivity between isothio-cyanate group of FITC and amino group was high; therefore, the peptides possessing many of amino group became our ideal choice. The other reason is that these peptides as a new carrier were developed in our group and have proved to be effective to embed dyes and image tumor tissues [41, 43].

PEG-PLL-PLLeu triblock copolymers were dissolved in water and simultaneously formed self-assembled micelles. CMC value for these copolymers was 79.4 mg/L by fluorescent method. Encapsulation efficiency (EE) and drug loading efficiency (LE) of the NPs are crucial for their application. Table S1 showed the EE or LE of the NPs formulations. EE and LE of RBLC were 66.5% and 4.7% when feed mass ratio for PEG-PLL-PLLeu-FITC to RBITC was 13.5. EE and LE was observed at 53.4% or 8.9% when feed mass ratio was 5.4. The hydrodynamic radius of DPNs was about 57 nm by DLS (Fig. 2C). DPNs showed

Nanoscale Accepted Manuscript

compact and spherical morphology with a diameter of 30-50 nm, demonstrated by transmission electronic microscopic (TEM) image (Fig. 2D). Zeta potential analysis of DPNs showed that the surface potential was about + 22.1 mV, which decreased compared to the blank micelle NPs assembled by PEG-PLL-PLLeu copolymers (about + 60 mV) [41], indicating that modification of FITC on the copolymers changed the surface potential of NPs. The morphology, size and zeta potential of RPNs were similar to DPNs (the data were not shown).The stability of micelles was evaluated by monitoring the particle size at room temperature for 6 weeks. The results showed that the sizes of the micelles in water did not significantly change within 5 weeks

pH response of the DPNs in solution

The pH response of DPNs was characterized by fluorometry with dual wavelength excitation in sodium phosphate buffers of various pH (3.5-9.3). The fluorescence emission peaked at 580 nm increased dramatically as the buffer pH decreasing (Fig. 3A), whereas the fluorescein emission centered at 520 nm decreased as the buffer pH lowered (Fig. 3B). The emission, with the spectrum identical to that of RBL, was ascribed to the formation of Rhodamine via acid mediated opening of Rhodamine-lactam in the nanoparticles.The fluorescence intensity of RBL at 580 nm in the nanoparticles was 55 fold brighter at pH 5.6 relative to pH 7.4. Since there was almost nonflurescence of RBL at physiological pH (pH 7.4) in the normal tissues or in the cytosol, thus our results indicated that DPNs was suitable for tumor tissue (pH 7.0-5.5) and lysosome acidity (pH 5.5-3.5).The dual fluorescence peaks were dramatically occured when pH value reduced to 4.2 via single-wavelength excitation (Fig. 3B), which indicated fluorescence resonance energy transfer (FRET) occured as the buffer pH decreased.

In addition, the effect of self-quenching of RBLC embedded in micelles core was considered. Since RBLC itself was no fluorescence at this situation, its self-quenching was not a problem at alkaline and neutral conditions. On the contrary, RBLC became hydrophilic and released from micells as well as emitted fluorescence at acidic environment by acid mediated opening of Rhodamine-lactam. Hence, self-quenching did not come up in this condition because RBLC become rhodamine and had been released from micelles.

The ratios between fluorescence emission intensity of RBLC at 580 nm ($I_{580\ nm}$) and intensity of fluorescein at 520 nm ($I_{520\ nm}$) were plotted vs. pH. The titration curves obtained from dual-wavelength excitation illustrating that subtle acidification in the range of pH 6.5-4.2 resulted in very large changes in intensity ratio (Fig. 3C). In contrast, previous fluorescein based sensors often exhibited moderate ratio changes (0.3-1) for a fluctuation of one pH unit [25, 44, 45]. The improved sensitivity could be attributed to the favorable inverse pH responses of RBL and fluorescein: RBLC demonstrated dramatically enhanced fluorescence upon acidification whereas the fluorescence of fluorescein decreased. Overlapping of the lysosome acidity range (pH 5.5-3.5) with the optimal sensing range of DPNs (pH 6.5-3.5) explored its potential applications for monitoring microenvironment of solid tumors and cellular lysosome acidity. Since many other ions such as Na^+, K^+ and Mg^{2+}, and chemically reactive species, e.g. HOCl and H_2O_2 existed in animal body and cells. Thus measuring the selectivity of DPNs toward H^+ was necessary. Fig. 3D showed that DPNs had distinct response to H^+ and exhibited negligible variety toward Na^+, K^+, Hg^+, Cu^{2+}, Fe^{2+}, Ca^{2+}, Mg^{2+}, Zn^{2+}, Mn^{2+}, Cd^{2+}, Sn^{2+}, Al^{3+}, Fe^{3+}, Co^{2+}, H_2O_2 or OCl^{-1} in water and cell culture medium.

pH response of the DPNs towards cells

The pH nanosensors of DPNs were very essential for intracellular pH measurements. The realtime monitoring of the cellular pH was performed. MCF-7 cells were pre-cultured with DPNs for 1 h in advance, then incubated at 37 °C for 15 min in high K^+ buffer with various pH values in the presence of 10 μM nigericin, which could homogenize the intracellular pH to that of the incubating buffers and culture medium [2]. The fluorescence images of MCF-7 cells were measured by CLSM. As shown in Fig. 4, the fluorescence intensity from the FITC channel (green) in cellsdeclined obviously with pH decreasing, whereas that from the RBITC channel (red) increased distinctly. At higher pH value (pH 7.4, pH .8.0), red fluorescence was barely visible (Fig. 4D and 4E). The colocalization of green and red fluorescence in the merge channel was obtained based on above two channels, displaying a characteristic pH-dependent signal change. The pH curve was constructed according to these fluorescence images, which showed the ratio signals between RBLC/FITC (I_{RBLC}/I_{FITC}) channel to pH range from 5.6 ～ 8.0 generated good linear calibration (Fig. 4F), implying that DPNs had an excellent pH response to cells *in vitro*.

Cellular lysosome is an acidic environment and lysosomal pH value is ranged from 3.5 to 5.0 [46, 47]. Since DPNs were inclined to internalizeinto cells by endocytosis and accumulated in lysosomes, it was possible to probe lysosomes using DPNs. Hela cells were stained with DPNs and LysoTracker Blue DND-22, which was a blue lysosome marker. Microscopic imagings analysis illustrated that red fluorescence was strong and the fluorescence of FITC in DPNs was partly quenched in cells (Fig. 5). Colocalization of Blue DND-22 with FITC and rodamine demonstrated that internalized DPNs were site-specifically delivered into lysosomes. strong red fluorescence manifested that acidic lysosome released RBLC and rodamine forming the ratio of $I_{rodamine}/I_{FITC}$ in inside cells was up to 4.5, impling the pH in lysosome would be about 4.0-5.0 in MCF-7 cells.

The cytotoxicity of DPNs and RPNs was evaluated in MCF-7 cells using MTT assay. As shown in Fig. 6, it was found that RPNs and DPNs micelles with 0.5-80 μg/mL caused over 5-30 % of cell death after 24 h incubation. The cytotoxicity of these NPs was similar to the blank PEG-PLL-PLLeu micelles refering to previous research [41], indicating the cytotoxicity of RPNs and DPNs mainly was derived from PEG-PLL-PLLeu copolymers. Considering low concentration (20 μg/mL) and relatively short incubating time (30 min) of RPNs and DPNs applied for pH indication, the cytotoxicity of micelles would not seriously influence in our experiments.

RPNs for contrast-enhanced *in vivo* cancer imaging

It was well established that solid tumors tend to have a more acidic microenvironment than normal tissues [8, 9]. The increase of hydrogen ion concentrationwas thought to be due to a combination of a more glycolytic phenotype, as well as reduced oxygen availability, leading to lactic acidosis from glycolysis [10]. A poor and chaotic tumor vascularization leads to the inefficient washout of the acidic products and contributes further to development of the chronically acidic extracellular environment [48].

The measurement with potentiometric microelectrode and magnetic resonance spectroscopy proved that the pHe of solid tumors in mice was about 6.0-7.0 [49-51]. a series of Gao group's

Nanoscale Accepted Manuscript

This journal is © The Royal Society of Chemistry [year]

work [52-54] had proved that it was possible for using pH activatable fluorescence nanoparticles to image tumour microenvironment. hence, it is reasonable and feasible using our probes to imaging tumor. Considering interfering of strong green autofluorescence of animal, RPNs were applied for the next experiments instead of DPNs. As shown in Fig. 7, eppendorf tubes loaded with RBL-NPs solution at different pH value (pH 5.6, pH 6.0, pH 6.5, pH 7.0, pH 7.4) looked almost identical in bright field image (Fig. 7A) while appeared obviously distinct in fluorescence image (Fig. 7B). In fact, red fluorescence intensity decreased when pH values increased stepwise from 5.6 to 7.4 and this situation would enable semi quantitative read-out by Maestro™ *in vivo* fluorescence imaging system (Fig. 7C).

To demonstrate the applicability of RPNs to imaging tumor, fluorescence imagings of anatomic tumor and organs were first employed using the Maestro™ *in vivo*. As shown in Fig. 8, there was a dramatically stronger fluorescence signals demonstrated on the anatomic tumor tissues than the other organs after the MCF-7 tumor-bearing nude mice was injected RPNs solutions for 2 h. Since RPNs itself has almost no fluorescence background signals in the environment of pH 7.4 and our previous work [43] had proved that the micelles accumulated in liver and kidneys were more than in tumor in 4 hours after I.V. injection. Hence, the enhancement of fluorescence signals in tumor tissues indicated RPNs could probe the difference between the tumor and other organs, where the pH microenviroment of tumor possibly lower than normal tissues. But unexpectedly, a whole animal fluorescence imaging almost could not make a distinction between tumor and other region (the data were not shown). In addition, the fluorescence spectra obtained from the tumor region before injection of RPNs almost overlapped with one obtained from the same tumor region after injection of RPNs, when using the same *in vivo* imaging system and the same imaging parameters (Fig. 8C). It indicated that high autofluorescence with wavelength from 500 nm to 600 nm originating from animal skin might be the critical factor that interfered with detection of RPNs fluorescent signals. Since fluorescence emission peak of rodamine at 580 nm was in the range of strong autofluorescence, it was difficult to distinguish the light by biological structures themselves from artificially adding fluorescent markers. We expected that the novel near infrared pH-activatable probes would be further designed for quantitatively monitoring the tumor pH fluctuations under different stimuli.

Conclusions

In summary, we synthetized DPNs and RPNs for pH sensing in living cells and tumor imaging. DPNs simultaneously was successfully packed with acid and base activable pH reporting dyes, which could act as highly sensitive ratiometric nanosensors for intracellular pH monitoring.The DPNs exhibited excellent pH sensitivity with a dynamic pH value ranging from 4.0 to 7.0, which was highly favorable to the quantitative analysis of intracellular pH changes. DPNs were further successfully used to monitor lysosomal pH value. Cell toxic studies have demonstrated their good biocompatibility. Moreover, RPNs were expected to distinguish the extracellular acidification of tumor tissue from normal tissue using fluorescence imaging. This work clearly showed that DPNs could serve as a promising platform for constructing practical fluorescent pH nanosensors.

Acknowledgements

The work was supported by the National Basic Research Program of China (973 program Grant No. 2011CB933600), the National Natural Science Foundation of China (Grant No. 21375141,Grant No. 81071249), Natural Science Foundation of Guangdong Province of China (Grant No. 9478922035-X003399), Shenzhen Key Laboratory of Cancer Nanotechnology (CXB201005250029A), Guangdong Innovation Reasearch Team of Low-cost Healthcare and Shenzhen Science and Technology Program (Grant No. JC201005260247A, CXB201005250029A, ZYC201105170305A, JCYJ20120615125829685).

Notes and references

Guangdong Key Laboratory of Nanomedicine, Shenzhen Key Laboratory of Cancer Nanotechnology, Institute of Biomedicine and Biotechnology, Shenzhen Institutes of Advanced Technology, Chinese Academy of Sciences, Shenzhen 518055 , Guangdong (P. R. China). Fax: +86 755 86392299; Tel: +86 755 86392210; E-mail: lt.cai@siat.ac.cn

† P. Gong & Y. Yang were contributed equally to this work

1 K. S. K. Gjetting, C. K. Ytting, A. Schulz and A. T. Fuglsang, *J. Exp. Bot.*, 2012, **63**, 3207-3218.

2 M. Tafani, J. A. Cohn, N. O. Karpinich, R. J. Rothman, M. A. Russo and J. L. Farber, *J. Biol. Chem.*, 2002, **277**, 49569-49576.

3 R. J. Gillies, R. Martinez-Zaguilan, E. P. Peterson and P. Perona, *Cell Physiol. Biochem.*, 1992, **2**, 159-179.

4 G. FitzHarris and J. M. Baltz, *Reproduction*, 2009, **138**, 619-627.

5 R. P. Henry and M. G. Wheatly, *Am. Zool.*, 1992, **32**, 407-416.

6 R. J. Coakley, C. Taggart, N. G. McElvaney and S. J. O'Neill, *Blood*, 2002, **100**, 3383-3391.

7 D. M. Prescott, H. C. Charles, J. M. Poulson, R. L. Page, D. E. Thrall, Z. Vujaskovic and M. W. Dewhirst, *Clin. Cancer Res.*, 2000, **6**, 2501-2505.

8 P. Vaupel, F. Kallinowski and P. Okunieff, *Cancer Res.*, 1989, **49**, 6449-6465.

9 J. L. Wikehooley, J. Haveman and H. S. Reinhold, *Radiother. Oncol.*, 1984, **2**, 343-366.

10 C. J. Gulledge and M. W. Dewhirst, *Anticancer Res.*, 1996, **16**, 741-749.

11 D. Fukumura, L. Xu, Y. Chen, T. Gohongi, B. Seed and R. K. Jain, *Cancer Res.*, 2001, **61**, 6020-6024.

12 E. K. Rofstad, B. Mathiesen, K. Kindem and K. Galappathi, *Cancer Res.*, 2006, **66**, 6699-6707.

13 L. Wang, X. Zhu, C. Xie, N. Ding, X. F. Weng, W. Y. Lu, X. B. Wei and C. Li, *Chem. Commun.*, 2012, **48**, 11677-11679.

14 I. F. Robey and N. K. Martin, *Bmc Cancer*, 2011, **11**.

15 1J. W. Wojtkowiak, D. Verduzco, K. J. Schramm and R. J. Gillies, *Mol. Pharm.*, 2011, **8**, 2032-2038.

16 W. Shi, X. H. Li and H. M. Ma, *Angew. Chem. Int. Ed. Engl.*, 2012, **51**, 6432-6435.

17 T. Awaji, A. Hirasawa, H. Shirakawa, G. Tsujimoto and S. Miyazaki, *Biochem. Biophys. Res. Commun.*, 2001, **289**, 457-462.

18 J. Y. Han and K. Burgess, *Chem. Rev.*, 2010, **110**, 2709-2728.

19 19. T. Myochin, K. Kiyose, K. Hanaoka, H. Kojima, T. Terai and T. Nagano, *J. Am. Chem. Soc.*, 2011, **133**, 3401-3409.

Nanoscale Accepted Manuscript

20 E. Nakata, Y. Yukimachi, Y. Nazumi, Y. Uto, H. Maezawa, T. Hashimoto, Y. Okamoto and H. Hori, *Chem. Commun.*, 2010, **46**, 3526-3528.

21 M. Tantama, Y. P. Hung and G. Yellen, *J. Am. Chem. Soc.*, 2011, **133**, 10034-10037.

22 B. Tang, F. Yu, P. Li, L. L. Tong, X. Duan, T. Xie and X. Wang, *J. Am. Chem. Soc.*, 2009, **131**, 3016-3023.

23 L. Yuan, W. Y. Lin and Y. M. Feng, *Org. Biomol. Chem.*, 2011, **9**, 1723-1726.

24 Y.-T. Tsai, J. Zhou, H. Weng, J. Shen, L. Tang and W.-J. Hu, *Adv. Healthc. Mater.*, 2013, n/a-n/a.

25 H. S. Peng, J. A. Stolwijk, L. N. Sun, J. Wegener and O. S. Wolfbeis, *Angew. Chem. Int. Ed. Engl.*, 2010, **49**, 4246-4249.

26 M. J. Marin, F. Galindo, P. Thomas and D. A. Russell, *Angew. Chem. Int. Ed. Engl.*, 2012, **51**, 9657-9661.

27 R. Guillet-Nicolas, A. Popat, J. L. Bridot, G. Monteith, S. Z. Qiao and F. Kleitz, *Angew. Chem. Int. Ed. Engl.*, 2013, **52**, 2318-2322.

28 Y. E. K. Lee, R. Smith and R. Kopelman, *Annu. Rev. Anal. Chem.*, 2009, **2**, 57-76.

29 S. Q. Wu, Z. Li, J. H. Han and S. F. Han, *Chem. Commun.*, 2011, **47**, 11276-11278.

30 K. Y. Niu, H. M. Zheng, Z. Q. Li, J. Yang, J. Sun and X. W. Du, *Angew. Chem. Int. Ed. Engl.*, 2011, **50**, 4099-4102.

31 Y. H. Chan, C. F. Wu, F. M. Ye, Y. H. Jin, P. B. Smith and D. T. Chiu, *Analytical Chemistry*, 2011, **83**, 1448-1455.

32 Z. M. Bhujwalla, C. L. McCoy, J. D. Glickson, R. J. Gillies and M. Stubbs, *Br. J. Cancer*, 1998, **78**, 606-611.

33 V. Estrella, T. A. Chen, M. Lloyd, J. Wojtkowiak, H. H. Cornnell, A. Ibrahim-Hashim, K. Bailey, Y. Balagurunathan, J. M. Rothberg, B. F. Sloane, J. Johnson, R. A. Gatenby and R. J. Gillies, *Cancer Res.*, 2013, **73**, 1524-1535.

34 M. Stubbs, P. M. J. McSheehy, J. R. Griffiths and C. L. Bashford, *Mol. Med. Today*, 2000, **6**, 15-19.

35 R. J. Gillies, Z. Liu and Z. Bhujwalla, *Am. J. Physiol.*, 1994, **267**, C195-C203.

36 T. Frenzel, S. Kossler, H. Bauer, U. Niedballa and H. J. Weinmann, *Invest. Radiol.*, 1994, **29**, S220-S222.

37 J. R. Griffiths, A. N. Stevens, R. A. Iles, R. E. Gordon and D. Shaw, *Biosci. Rep.*, 1981, **1**, 319-325.

38 D. A. Rottenberg, J. Z. Ginos, K. J. Kearfott, L. Junck and D. D. Bigner, *Ann. Neurol.*, 1984, **15**, S98-S102.

39 D. P. William H. Daly, *Tetrahedron Lett.*, 1988, **29**, 4.

40 C. H. Wang, S. Leffler, D. H. Thompson and C. A. Hrycyna, *Biochem. Biophys. Res. Commun.*, 2005, **331**, 351-356.

41 J. Z. Deng, N. N. Gao, Y. A. Wang, H. Q. Yi, S. T. Fang, Y. F. Ma and L. T. Cai, *Biomacromolecules*, 2012, **13**, 3795-3804.

42 A. Mehreteab and B. Chen, *J. Am. Oil Chem. Soc.*, 1995, **72**, 49-52.

43 L. Wu, S. Fang, S. Shi, J. Deng, B. Liu and L. Cai, Biomacromolecules, 2013, 14, 3027–3033.

44 T. Jin, A. Sasaki, M. Kinjo and J. Miyazaki, *Chem. Commun.*, 2010, **46**, 2408-2410.

45 J. Lei, L. Wang and J. Zhang, *Chem. Commun.*, 2010, **46**, 8445-8447.

46 M. J. Geisow, P. D. Hart and M. R. Young, *J. Cell Biol.*, 1981, **89**, 645-652.

47 K. Glunde, S. E. Guggino, M. Solaiyappan, A. P. Pathak, Y. Ichikawa and Z. M. Bhujwalla, *Neoplasia*, 2003, **5**, 533-545.

48 L. E. Gerweck and K. Seetharaman, *Cancer Res.*, 1996, **56**, 1194-1198.

49 D. Shweiki, M. Neeman, A. Itin and E. Keshet, *Proc. Natl. Acad. Sci. U. S. A.*, 1995, **92**, 768-772.

50 N. Weidner, J. P. Semple, W. R. Welch and J. Folkman, *N. Engl. J. Med.*, 1991, **324**, 1-8.

51 E. R. Horak, R. Leek, N. Klenk, S. Lejeune, K. Smith, N. Stuart, M. Greenall, K. Stepniewska and A. L. Harris, *Lancet*, 1992, **340**, 1120-1124.

52 K. J. Zhou, H. M. Liu, S. R. Zhang, X. N. Huang, Y. G. Wang, G. Huang, B. D. Sumer and J. M. Gao, *J. Am. Chem. Soc.*, 2012, **134**, 7803-7811.

53 X. Huang, G. Huang, S. Zhang, K. Sagiyama, O. Togao, X. Ma, Y. Wang, Y. Li, T. C. Soesbe, B. D. Sumer, M. Takahashi, A. D. Sherry and J. Gao, *Angew. Chem. Int. Ed. Engl.*, 2013, **52**, 8074-8078.

54 Y. Wang, K. Zhou, G. Huang, C. Hensley, X. Huang, X. Ma, T. Zhao, B. D. Sumer, R. J. DeBerardinis and J. Gao, *Nat Mater*, 2014, **13**, 204-212.

Nanoscale Accepted Manuscript

This journal is © The Royal Society of Chemistry [year]

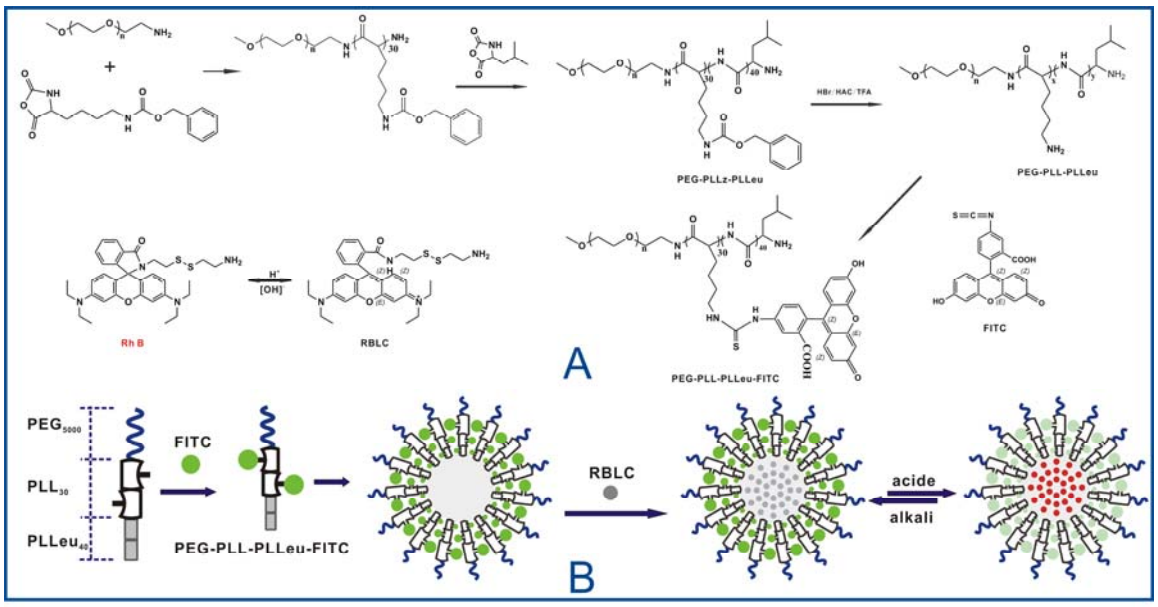

Fig 1. Synthesis of PEG-PLL-PLLeu Copolymers and PEG-PLL-PLLeu-FITC (A) and the Formation of DPNs and their response to pH (B).

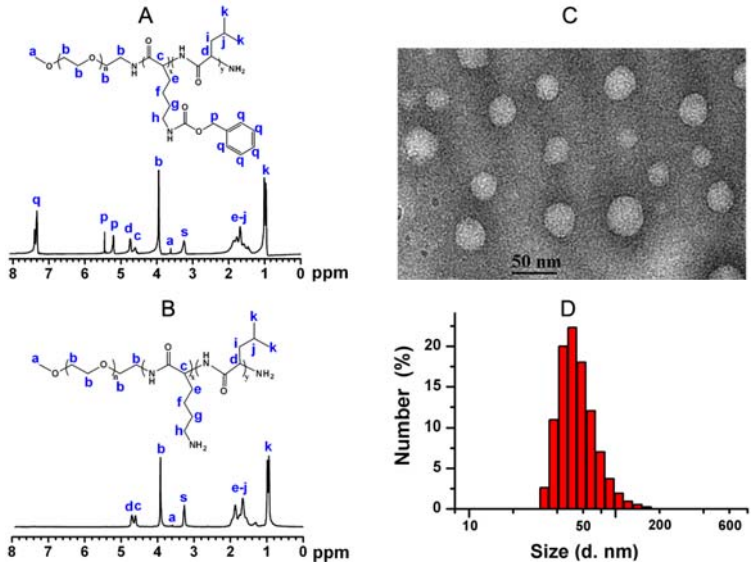

Fig. 2. Characterization of micelle NPs. ^{1}H NMR spectrum of PEG-PLLZ-PLLeu (A) and PEG-PLL-PLLeu (B) copolymers; (C) TEM image of DPNs; (D) Size distribution of DPNs by dynamic light scattering.

Nanoscale Accepted Manuscript

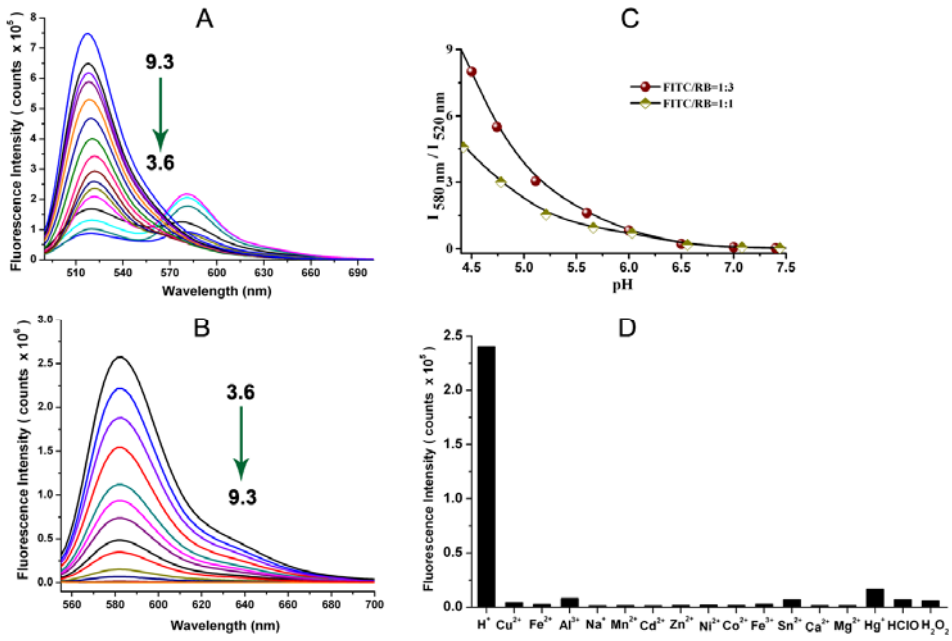

Fig. 3. Response of DPNs to pH. Fluorescence emission spectra of DPNs at different pH (9.3, 9.0, 8.5, 8.0, 7.4, 7.0, 6.5, 6.0, 5.6, 5.1, 4.7, 4.5, 4.2, 4.0, 3.8, 3.6) under dual wavelength excitation for FITC (λ_{ex} at 488 nm) (A) and for RBLC (λ_{ex} at 550 nm) (B); (C) pH titration curves of RBL-FITC-NPs from dual-wavelength excitation with different concentration ratio of RBL and FITC; (D) selectivity of RBL-FITC-NPs in water for H^+ with other ions (λ_{ex} at 488 nm, λ_{ex} at 550 nm).

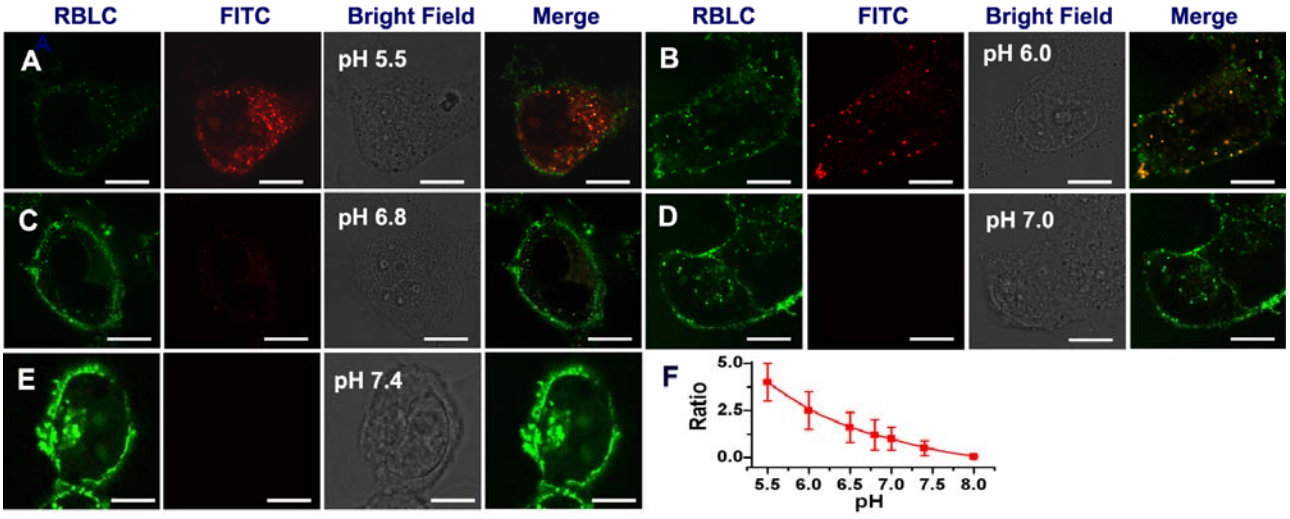

Fig. 4. Fluorescent images of MCF-7 cells clamped at pH 5.5 (A), 6.0 (B), 6.8 (C), 7.0 (D) and 7.4 (E) after incubation with DPNs, respectively. The images of FITC channel and RBLC channel were excited at 488nm and 543nm, respectively, and collected in the ranges of 500–540 nm and 560–610 nm, respectively. Bars, 10 μm. (F) pH calibration curve of DPNs.

Nanoscale Accepted Manuscript

This journal is © The Royal Society of Chemistry [year]

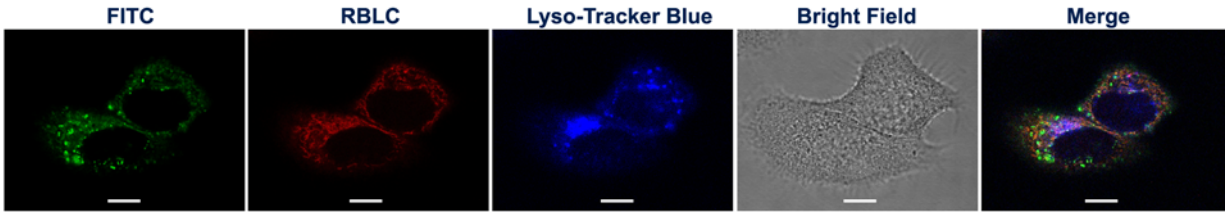

Fig. 5. Intracellular distributions of DPNs as compared to LysoTracker Blue DND-22. The images of FITC channel, RBLC channel and Lyso-Tracker Blue channel, were excited at 488nm, 543nm and 405 nm, respectively, and collected in the ranges of 500–540 nm, 560–610 nm and 420–480 nm, respectively. Bars, 10 μm. Bars, 10 μm.

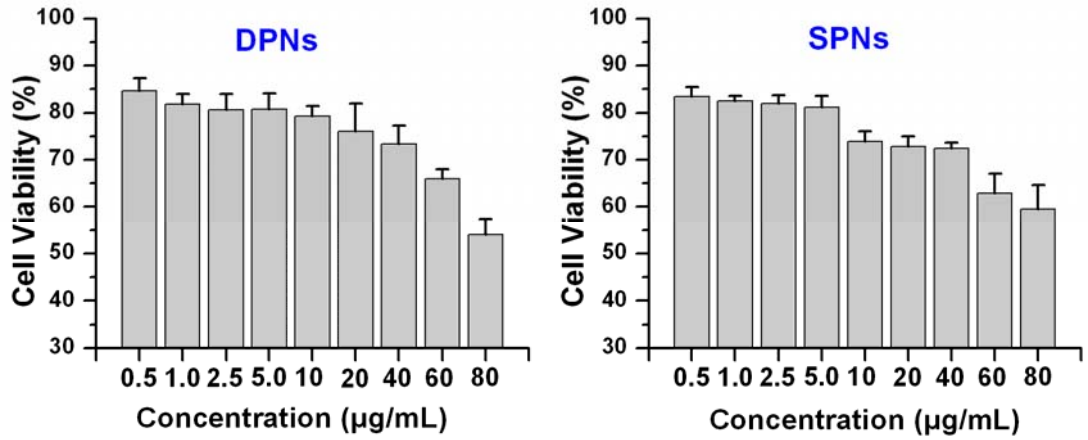

Fig. 6. Cell viability of MCF-7 cells treated with DPNs or SPNs *in vitro*. The of MCF-7 cells were cultured with 0.5 to 80 μg/mL of DPNs or SPNs for 24 h, and the cell viability was measured by MTT assay.

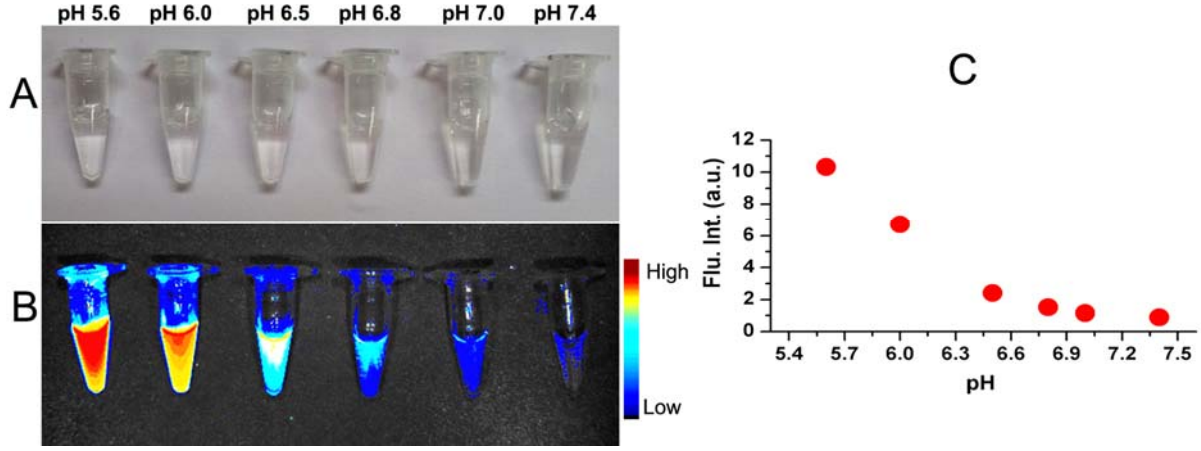

Fig. 7. Bright field (A) and fluorescence (B) images of RPNs in sodium phosphate buffer at pH5.6, 6.0, 6.5, 6.8, 7.0 and 7.4 in eppendorf tubes. For fluorescence image, 523 nm (±25 nm) bandpass filter and a 560 nm longpass filter (560 to 740 nm) were selected to be used as the excitation filter and the emission filter, respectively. (C) pH calibration curve of RPNs.

Nanoscale Accepted Manuscript

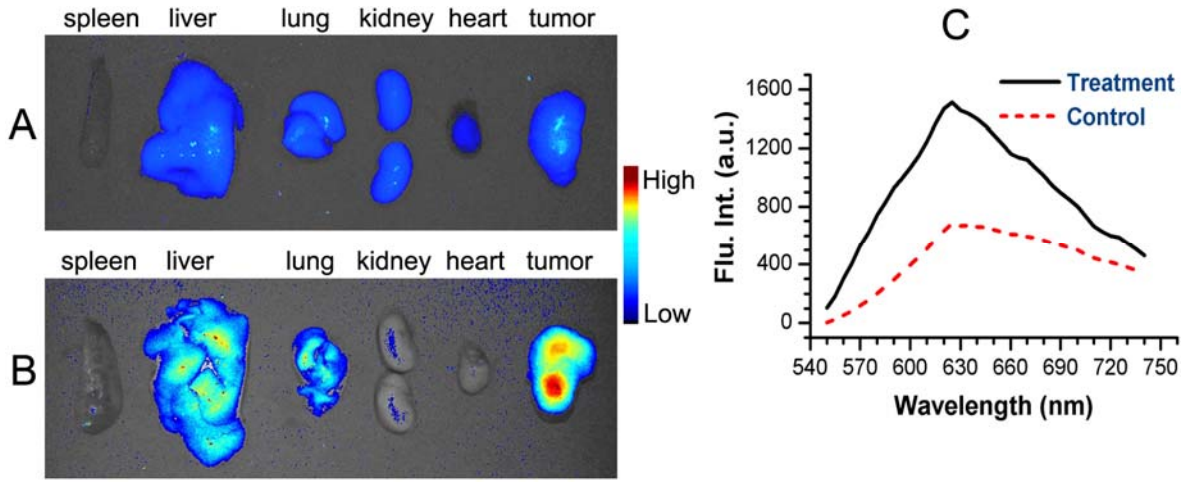

Fig. 8. Fluoresncence imagings of anatomic tumor and organs of nude mice injected without (A) or with (B) RPNs. A 523 nm (±25 nm) bandpass filter and a 560 nm longpass filter (560 to 740 nm) were selected to be used as the excitation filter and the emission filter, respectively. (C) the fluorescence spectra obtained from the tumor region before and after injection of RPNs using an *in vivo* imaging system.

Nanoscale Accepted Manuscript

This journal is © The Royal Society of Chemistry [year]